

Directional limits on persistent gravitational waves using LIGO S5 science data

J. Abadie²⁹, B. P. Abbott²⁹, R. Abbott²⁹, M. Abernathy⁶⁶, T. Accadia²⁷, F. Acernese^{19ac}, C. Adams³¹, R. Adhikari²⁹, P. Ajith²⁹, B. Allen^{2,78}, G. S. Allen⁵², E. Amador Ceron⁷⁸, R. S. Amin³⁴, S. B. Anderson²⁹, W. G. Anderson⁷⁸, F. Antonucci^{22a}, M. A. Arain⁶⁵, M. C. Araya²⁹, M. Aronsson²⁹, K. G. Arun²⁶, Y. Aso²⁹, S. M. Aston⁶⁴, P. Astone^{22a}, D. Atkinson³⁰, P. Aufmuth²⁸, C. Aulbert², S. Babak¹, P. Baker³⁷, G. Ballardin¹³, S. Ballmer²⁹, D. Barker³⁰, S. Barnum³², F. Barone^{19ac}, B. Barr⁶⁶, P. Barriga⁷⁷, L. Barsotti³², M. Barsuglia⁴, M. A. Barton³⁰, I. Bartos¹², R. Bassiri⁶⁶, M. Bastarrika⁶⁶, J. Bauchrowitz², Th. S. Bauer^{41a}, B. Behnke¹, M.G. Beker^{41a}, A. Bellettoile²⁷, M. Benacquista⁵⁹, A. Bertolini², J. Betzwieser²⁹, N. Beveridge⁶⁶, P. T. Beyersdorf⁴⁸, S. Bigotta^{21ab}, I. A. Bilenko³⁸, G. Billingsley²⁹, J. Birch³¹, S. Birindelli^{43a}, R. Biswas⁷⁸, M. Bitossi^{21a}, M. A. Bizouard^{26a}, E. Black²⁹, J. K. Blackburn²⁹, L. Blackburn³², D. Blair⁷⁷, B. Bland³⁰, M. Blom^{41a}, C. Boccara^{26b}, O. Bock², T. P. Bodiya³², R. Bondarescu⁵⁴, F. Bondu^{43b}, L. Bonelli^{21ab}, R. Bonnand³³, R. Bork²⁹, M. Born², S. Bose⁷⁹, L. Bosi^{20a}, B. Bouhou⁴, M. Boyle⁸, S. Braccini^{21a}, C. Bradaschia^{21a}, P. R. Brady⁷⁸, V. B. Braginsky³⁸, J. E. Brau⁷¹, J. Breyer², D. O. Bridges³¹, A. Brillet^{43a}, M. Brinkmann², V. Brisson^{26a}, M. Britzger², A. F. Brooks²⁹, D. A. Brown⁵³, R. Budzyński^{45b}, T. Bulik^{45cd}, H. J. Bulten^{41ab}, A. Buonanno⁶⁷, J. Burguet-Castell⁷⁸, O. Burmeister², D. Buskulic²⁷, C. Buy⁴, R. L. Byer⁵², L. Cadonati⁶⁸, G. Cagnoli^{17a}, J. Cain⁵⁶, E. Calloni^{19ab}, J. B. Camp³⁰, E. Campagna^{17ab}, P. Campsie⁶⁶, J. Cannizzo³⁹, K. Cannon²⁹, B. Canuel¹³, J. Cao⁶¹, C. Capano⁵³, F. Carbognani¹³, S. Caride⁶⁹, S. Caudill³⁴, M. Cavaglià⁵⁶, F. Cavalier^{26a}, R. Cavalieri¹³, G. Cella^{21a}, C. Cepeda²⁹, E. Cesarini^{17b}, T. Chalermongsak²⁹, E. Chalkley⁶⁶, P. Charlton¹¹, E. Chassande-Mottin⁴, S. Chelkowski⁶⁴, Y. Chen⁸, A. Chincarini¹⁸, N. Christensen¹⁰, S. S. Y. Chua⁵, C. T. Y. Chung⁵⁵, D. Clark⁵², J. Clark⁹, J. H. Clayton⁷⁸, F. Cleva^{43a}, E. Coccia^{23ab}, C. N. Colacino^{21ab}, J. Colas¹³, A. Colla^{22ab}, M. Colombini^{22b}, R. Conte⁷³, D. Cook³⁰, T. R. Corbitt³², N. Cornish³⁷, A. Corsi^{22a}, C. A. Costa³⁴, J.-P. Coulon^{43a}, D. M. Coward⁷⁷, D. C. Coyne²⁹, J. D. E. Creighton⁷⁸, T. D. Creighton⁵⁹, A. M. Cruise⁶⁴, R. M. Culter⁶⁴, A. Cumming⁶⁶, L. Cunningham⁶⁶, E. Cuoco¹³, K. Dahl², S. L. Danilishin³⁸, R. Dannenberg²⁹, S. D'Antonio^{23a}, K. Danzmann^{2,28}, K. Das⁶⁵, V. Dattilo¹³, B. Daudert²⁹, M. Davier^{26a}, G. Davies⁹, A. Davis¹⁴, E. J. Daw⁵⁷, R. Day¹³, T. Dayanga⁷⁹, R. De Rosa^{19ab}, D. DeBra⁵², J. Degallaix², M. del Prete^{21ac}, V. Dergachev²⁹, R. DeRosa³⁴, R. DeSalvo²⁹, P. Devanka⁹, S. Dhurandhar²⁵, L. Di Fiore^{19a}, A. Di Lieto^{21ab}, I. Di Palma², M. Di Paolo Emilio^{23ac}, A. Di Virgilio^{21a}, M. Díaz⁵⁹, A. Dietz²⁷, F. Donovan³², K. L. Dooley⁶⁵, E. E. Doomes⁵¹, S. Dorsher⁷⁰, E. S. D. Douglas³⁰, M. Drago^{44cd}, R. W. P. Drever⁶, J. C. Driggers²⁹, J. Dueck², J.-C. Dumas⁷⁷, T. Eberle², M. Edgar⁶⁶, M. Edwards⁹, A. Effler³⁴, P. Ehrens²⁹, R. Engel²⁹, T. Etzel²⁹, M. Evans³², T. Evans³¹, V. Fafone^{23ab}, S. Fairhurst⁹, Y. Fan⁷⁷, B. F. Farr⁴², D. Fazi⁴², H. Fehrmann², D. Feldbaum⁶⁵, I. Ferrante^{21ab}, F. Fidecaro^{21ab}, L. S. Finn⁵⁴, I. Fiori¹³, R. Flaminio³³, M. Flanigan³⁰, K. Flasch⁷⁸, S. Foley³², C. Forrest⁷², E. Forsi³¹, N. Fotopoulos⁷⁸, J.-D. Fournier^{43a}, J. Franc³³, S. Frasca^{22ab}, F. Frasconi^{21a}, M. Frede², M. Frei⁵⁸, Z. Frei¹⁵, A. Freise⁶⁴, R. Frey⁷¹, T. T. Fricke³⁴, D. Friedrich², P. Fritschel³², V. V. Frolov³¹, P. Fulda⁶⁴, M. Fyffe³¹, M. Galimberti³³, L. Gammaitoni^{20ab}, J. A. Garofoli⁵³, F. Garufi^{19ab}, G. Gemme¹⁸, E. Genin¹³, A. Gennai^{21a}, I. Gholami¹, S. Ghosh⁷⁹, J. A. Giaime^{34,31}, S. Giampaonis², K. D. Giardina³¹, A. Giazotto^{21a}, C. Gill⁶⁶, E. Goetz⁶⁹, L. M. Goggin⁷⁸, G. González³⁴, M. L. Gorodetsky³⁸, S. Goßler², R. Gouaty²⁷, C. Graef², M. Granata⁴, A. Grant⁶⁶, S. Gras⁷⁷, C. Gray³⁰, R. J. S. Greenhalgh⁴⁷, A. M. Gretarsson¹⁴, C. Greverie^{43a}, R. Grossi⁵⁹, H. Grote², S. Grunewald¹, G. M. Guidi^{17ab}, E. K. Gustafson²⁹, R. Gustafson⁶⁹, B. Hage²⁸, P. Hall⁹, J. M. Hallam⁶⁴, D. Hammer⁷⁸, G. Hammond⁶⁶, J. Hanks³⁰, C. Hanna²⁹, J. Hanson³¹, J. Harms⁶, G. M. Harry³², I. W. Harry⁹, E. D. Harstad⁷¹, K. Haughian⁶⁶, K. Hayama⁴⁰, J.-F. Hayau^{43b}, T. Hayler⁴⁷, J. Heefner²⁹, H. Heitmann⁴³, P. Hello^{26a}, I. S. Heng⁶⁶, A. W. Heptonstall²⁹, M. Hewitson², S. Hild⁶⁶, E. Hirose⁵³, D. Hoak⁶⁸, K. A. Hodge²⁹, K. Holt³¹, D. J. Hosken⁶³, J. Hough⁶⁶, E. J. Howell⁷⁷, D. Hoyland⁶⁴, D. Huet¹³, B. Hughey³², S. Husa⁶², S. H. Huttner⁶⁶, T. Huynh-Dinh³¹, D. R. Ingram³⁰, R. Inta⁵, T. Isogai¹⁰, A. Ivanov²⁹, P. Jaradowski^{45e}, W. W. Johnson³⁴, D. I. Jones⁷⁵, G. Jones⁹, R. Jones⁶⁶, L. Ju⁷⁷, P. Kalmus²⁹, V. Kalogera⁴², S. Kandhasamy⁷⁰, J. B. Kanner⁶⁷, E. Katsavounidis³², K. Kawabe³⁰, S. Kawamura⁴⁰, F. Kawazoe², W. Kells²⁹, D. G. Keppel²⁹, A. Khalaidovski², F. Y. Khalili³⁸, E. A. Khazanov²⁴, H. Kim², P. J. King²⁹, D. L. Kinzel³¹, J. S. Kissel³⁴, S. Klimenko⁶⁵, V. Kondrashov²⁹, R. Kopparapu⁵⁴, S. Koranda⁷⁸, I. Kowalska^{45c}, D. Kozak²⁹, T. Krause⁵⁸, V. Kringel², S. Krishnamurthy⁴², B. Krishnan¹, A. Królak^{45af}, G. Kuehn², J. Kullman², R. Kumar⁶⁶, P. Kwee²⁸, M. Landry³⁰, M. Lang⁵⁴, B. Lantz⁵², N. Lastzka², A. Lazzarini²⁹, P. Leaci¹, J. Leong², I. Leonor⁷¹, N. Leroy^{26a}, N. Letendre²⁷, J. Li⁵⁹, T. G. F. Li^{41a}, N. Liguori^{44ab}, H. Lin⁶⁵, P. E. Lindquist²⁹, N. A. Lockerbie⁷⁶, D. Lodhia⁶⁴, M. Lorenzini^{17a}, V. Loriette^{26b}, M. Lormand³¹, G. Losurdo^{17a}, P. Lu⁵², J. Luan⁸, M. Lubinski³⁰, A. Lucianetti⁶⁵,

H. Lück^{2,28}, A. D. Lundgren⁵³, B. Machenschalk², M. MacInnis³², M. Mageswaran²⁹, K. Mailand²⁹, E. Majorana^{22a}, C. Mak²⁹, I. Maksimovic^{26b}, N. Man^{43a}, I. Mandel⁴², V. Mandic⁷⁰, M. Mantovani^{21ac}, F. Marchesoni^{20a}, F. Marion²⁷, S. Márka¹², Z. Márka¹², E. Maros²⁹, J. Marque¹³, F. Martelli^{17ab}, I. W. Martin⁶⁶, R. M. Martin⁶⁵, J. N. Marx²⁹, K. Mason³², A. Masserot²⁷, F. Matichard³², L. Matone¹², R. A. Matzner⁵⁸, N. Mavalvala³², R. McCarthy³⁰, D. E. McClelland⁵, S. C. McGuire⁵¹, G. McIntyre²⁹, G. McIvor⁵⁸, D. J. A. McKeehan⁹, G. Meadors⁶⁹, M. Mehmet², T. Meier²⁸, A. Melatos⁵⁵, A. C. Melissinos⁷², G. Mendell³⁰, D. F. Menéndez⁵⁴, R. A. Mercer⁷⁸, L. Merill⁷⁷, S. Meshkov²⁹, C. Messenger², M. S. Meyer³¹, H. Miao⁷⁷, C. Michel³³, L. Milano^{19ab}, J. Miller⁶⁶, Y. Minenkov^{23a}, Y. Mino⁸, S. Mitra²⁹, V. P. Mitrofanov³⁸, G. Mitselmakher⁶⁵, R. Mittelman³², B. Moe⁷⁸, M. Mohan¹³, S. D. Mohanty⁵⁹, S. R. P. Mohapatra⁶⁸, D. Moraru³⁰, J. Moreau^{26b}, G. Moreno³⁰, N. Morgado³³, A. Morgia^{23ab}, T. Morioka⁴⁰, K. Mors², S. Mosca^{19ab}, V. Moscatelli^{22a}, K. Mossavi², B. Mouris²⁷, C. M. Mow-Lowry⁵, G. Mueller⁶⁵, S. Mukherjee⁵⁹, A. Mullavey⁵, H. Müller-Ebhardt², J. Munch⁶³, P. G. Murray⁶⁶, T. Nash²⁹, R. Nawrodt⁶⁶, J. Nelson⁶⁶, I. Neri^{20ab}, G. Newton⁶⁶, A. Nishizawa⁴⁰, F. Nocera¹³, D. Nolting³¹, E. Ochsner⁶⁷, J. O'Dell⁴⁷, G. H. Ogin²⁹, R. G. Oldenburg⁷⁸, B. O'Reilly³¹, R. O'Shaughnessy⁵⁴, C. Osthelder²⁹, D. J. Ottaway⁶³, R. S. Ottens⁶⁵, H. Overmier³¹, B. J. Owen⁵⁴, A. Page⁶⁴, G. Pagliaroli^{23ac}, L. Palladino^{23ac}, C. Palomba^{22a}, Y. Pan⁶⁷, C. Pankow⁶⁵, F. Paoletti^{21a,13}, M. A. Papa^{1,78}, S. Pardi^{19ab}, M. Pareja², M. Parisi^{19b}, A. Pasqualetti¹³, R. Passaquieti^{21ab}, D. Passuello^{21a}, P. Patel²⁹, D. Pathak⁹, M. Pedraza²⁹, L. Pekowsky⁵³, S. Penn¹⁶, C. Peralta¹, A. Perreca⁶⁴, G. Persichetti^{19ab}, M. Pichot^{43a}, M. Pickenpack², F. Piergiovanni^{17ab}, M. Pietka^{45e}, L. Pinard³³, I. M. Pinto⁷⁴, M. Pitkin⁶⁶, H. J. Pletsch², M. V. Plissi⁶⁶, R. Poggiani^{21ab}, F. Postiglione⁷³, M. Prato¹⁸, V. Predoi⁹, L. R. Price⁷⁸, M. Prijatelj², M. Principe⁷⁴, R. Prix², G. A. Prodi^{44ab}, L. Prokhorov³⁸, O. Puncken², M. Punturo^{20a}, P. Puppo^{22a}, V. Quetschke⁵⁹, F. J. Raab³⁰, D. S. Rabeling^{41ab}, T. Radke¹, H. Radkins³⁰, P. Raffai¹⁵, M. Rakhamanov⁵⁹, B. Rankins⁵⁶, P. Rapagnani^{22ab}, V. Raymond⁴², V. Re^{44ab}, C. M. Reed³⁰, T. Reed³⁵, T. Regimbau^{43a}, S. Reid⁶⁶, D. H. Reitze⁶⁵, F. Ricci^{22ab}, R. Riesen³¹, K. Riles⁶⁹, P. Roberts³, N. A. Robertson^{29,66}, F. Robinet^{26a}, C. Robinson⁹, E. L. Robinson¹, A. Rocchi^{23a}, S. Roddy³¹, C. Röver², L. Rolland²⁷, J. Rollins¹², J. D. Romano⁵⁹, R. Romano^{19ac}, J. H. Romie³¹, D. Rosińska^{45g}, S. Rowan⁶⁶, A. Rüdiger², P. Ruggi¹³, K. Ryan³⁰, S. Sakata⁴⁰, F. Sakosky³⁰, F. Salemi², L. Sammut⁵⁵, L. Sancho de la Jordana⁶², V. Sandberg³⁰, V. Sannibale²⁹, L. Santamaría¹, G. Santostasi³⁶, S. Saraf⁴⁹, B. Sassolas³³, B. S. Sathyaprakash⁹, S. Sato⁴⁰, M. Satterthwaite⁵, P. R. Saulson⁵³, R. Savage³⁰, R. Schilling², R. Schnabel², R. M. S. Schofield⁷¹, B. Schulz², B. F. Schutz^{1,9}, P. Schwinberg³⁰, J. Scott⁶⁶, S. M. Scott⁵, A. C. Searle²⁹, F. Seifert²⁹, D. Sellers³¹, A. S. Sengupta²⁹, D. Sentenac¹³, A. Sergeev²⁴, D. A. Shaddock⁵, B. Shapiro³², P. Shawhan⁶⁷, D. H. Shoemaker³², A. Sibley³¹, X. Siemens⁷⁸, D. Sigg³⁰, A. Singer²⁹, A. M. Sintes⁶², G. Skelton⁷⁸, B. J. J. Slagmolen⁵, J. Slutsky³⁴, J. R. Smith⁷, M. R. Smith²⁹, N. D. Smith³², K. Somiya⁸, B. Sorazu⁶⁶, F. C. Speirits⁶⁶, L. Sperandio^{23ab}, A. J. Stein³², L. C. Stein³², S. Steinelechner², S. Steplewski⁷⁹, A. Stochino²⁹, R. Stone⁵⁹, K. A. Strain⁶⁶, S. Strigin³⁸, A. S. Stroeer³⁹, R. Sturani^{17ab}, A. L. Stuver³¹, T. Z. Summerscales³, M. Sung³⁴, S. Susmithan⁷⁷, P. J. Sutton⁹, B. Swinkels¹³, G. P. Szokoly¹⁵, D. Talukder⁷⁹, D. B. Tanner⁶⁵, S. P. Tarabrin², J. R. Taylor², R. Taylor²⁹, P. Thomas³⁰, K. A. Thorne³¹, K. S. Thorne⁸, E. Thrane^{70,a} and A. Thüring²⁸, C. Titsler⁵⁴, K. V. Tokmakov^{66,76}, A. Toncelli^{21ab}, M. Tonelli^{21ab}, O. Torre^{21ac}, C. Torres³¹, C. I. Torrie^{29,66}, E. Tournefier²⁷, F. Travassos^{20ab}, G. Traylor³¹, M. Trias⁶², J. Trummer²⁷, K. Tseng⁵², L. Turner²⁹, D. Ugolini⁶⁰, K. Urbanek⁵², H. Vahlbruch²⁸, B. Vaishnav⁵⁹, G. Vajente^{21ab}, M. Vallisneri⁸, J. F. J. van den Brand^{41ab}, C. Van Den Broeck⁹, S. van der Putten^{41a}, M. V. van der Sluys⁴², A. A. van Veggel⁶⁶, S. Vass²⁹, R. Vaulin⁷⁸, M. Vavoulidis^{26a}, A. Vecchio⁶⁴, G. Vedovato^{44c}, J. Veitch⁹, P. J. Veitch⁶³, C. Veltkamp², D. Verkindt²⁷, F. Vetrano^{17ab}, A. Viceré^{17ab}, A. E. Villar²⁹, J.-Y. Vinet^{43a}, H. Vocca^{20a}, C. Vorwick³⁰, S. P. Vyachanin³⁸, S. J. Waldman³², L. Wallace²⁹, A. Wanner², R. L. Ward²⁹, M. Was^{26a}, P. Wei⁵³, M. Weinert², A. J. Weinstein²⁹, R. Weiss³², L. Wen^{8,77}, S. Wen³⁴, P. Wessels², M. West⁵³, T. Westphal², K. Wette⁵, J. T. Whelan⁴⁶, S. E. Whitcomb²⁹, D. White⁵⁷, B. F. Whiting⁶⁵, C. Wilkinson³⁰, P. A. Willems²⁹, L. Williams⁶⁵, B. Willke^{2,28}, L. Winkelmann², W. Winkler², C. C. Wipf³², A. G. Wiseman⁷⁸, G. Woan⁶⁶, R. Wooley³¹, J. Worden³⁰, I. Yakushin³¹, H. Yamamoto²⁹, K. Yamamoto², D. Yeaton-Massey²⁹, S. Yoshida⁵⁰, P. Yu⁷⁸, M. Yvert²⁷, M. Zanolini¹⁴, L. Zhang²⁹, Z. Zhang⁷⁷, C. Zhao⁷⁷, N. Zotov³⁵, M. E. Zucker³², J. Zweizig²⁹

¹Albert-Einstein-Institut, Max-Planck-Institut für Gravitationsphysik, D-14476 Golm, Germany

²Albert-Einstein-Institut, Max-Planck-Institut für Gravitationsphysik, D-30167 Hannover, Germany

³Andrews University, Berrien Springs, MI 49104 USA

⁴Laboratoire AstroParticule et Cosmologie (APC) Université Paris Diderot,

CNRS: IN2P3, CEA: DSM/IRFU, Observatoire de Paris 10,

rue A.Domon et L.Duquet, 75013 Paris - France

⁵Australian National University, Canberra, 0200, Australia

- ⁶California Institute of Technology, Pasadena, CA 91125, USA
⁷California State University Fullerton, Fullerton CA 92831 USA
⁸Caltech-CaRT, Pasadena, CA 91125, USA
⁹Cardiff University, Cardiff, CF24 3AA, United Kingdom
¹⁰Carleton College, Northfield, MN 55057, USA
¹¹Charles Sturt University, Wagga Wagga, NSW 2678, Australia
¹²Columbia University, New York, NY 10027, USA
¹³European Gravitational Observatory (EGO), I-56021 Cascina (PI), Italy
¹⁴Embry-Riddle Aeronautical University, Prescott, AZ 86301 USA
¹⁵Eötvös Loránd University, Budapest, 1117 Hungary
¹⁶Hobart and William Smith Colleges, Geneva, NY 14456, USA
¹⁷INFN, Sezione di Firenze, I-50019 Sesto Fiorentino^a; Università degli Studi di Urbino 'Carlo Bo', I-61029 Urbino^b, Italy
¹⁸INFN, Sezione di Genova; I-16146 Genova, Italy
¹⁹INFN, Sezione di Napoli^a; Università di Napoli 'Federico II'^b Complesso Universitario di Monte S.Angelo, I-80126 Napoli; Università di Salerno, Fisciano, I-84084 Salerno^c, Italy
²⁰INFN, Sezione di Perugia^a; Università di Perugia^b, I-06123 Perugia, Italy
²¹INFN, Sezione di Pisa^a; Università di Pisa^b; I-56127 Pisa; Università di Siena, I-53100 Siena^c, Italy
²²INFN, Sezione di Roma^a; Università 'La Sapienza'^b, I-00185 Roma, Italy
²³INFN, Sezione di Roma Tor Vergata^a; Università di Roma Tor Vergata, I-00133 Roma^b; Università dell'Aquila, I-67100 L'Aquila^c, Italy
²⁴Institute of Applied Physics, Nizhny Novgorod, 603950, Russia
²⁵Inter-University Centre for Astronomy and Astrophysics, Pune - 411007, India
²⁶LAL, Université Paris-Sud, IN2P3/CNRS, F-91898 Orsay^a; ESPCI, CNRS, F-75005 Paris^b, France
²⁷Laboratoire d'Annecy-le-Vieux de Physique des Particules (LAPP), Université de Savoie, CNRS/IN2P3, F-74941 Annecy-Le-Vieux, France
²⁸Leibniz Universität Hannover, D-30167 Hannover, Germany
²⁹LIGO - California Institute of Technology, Pasadena, CA 91125, USA
³⁰LIGO - Hanford Observatory, Richland, WA 99352, USA
³¹LIGO - Livingston Observatory, Livingston, LA 70754, USA
³²LIGO - Massachusetts Institute of Technology, Cambridge, MA 02139, USA
³³Laboratoire des Matériaux Avancés (LMA), IN2P3/CNRS, F-69622 Villeurbanne, Lyon, France
³⁴Louisiana State University, Baton Rouge, LA 70803, USA
³⁵Louisiana Tech University, Ruston, LA 71272, USA
³⁶McNeese State University, Lake Charles, LA 70609 USA
³⁷Montana State University, Bozeman, MT 59717, USA
³⁸Moscow State University, Moscow, 119992, Russia
³⁹NASA/Goddard Space Flight Center, Greenbelt, MD 20771, USA
⁴⁰National Astronomical Observatory of Japan, Tokyo 181-8588, Japan
⁴¹Nikhef, National Institute for Subatomic Physics, P.O. Box 41882, 1009 DB Amsterdam^a; VU University Amsterdam, De Boelelaan 1081, 1081 HV Amsterdam^b, The Netherlands
⁴²Northwestern University, Evanston, IL 60208, USA
⁴³Université Nice-Sophia-Antipolis, CNRS, Observatoire de la Côte d'Azur, F-06304 Nice^a; Institut de Physique de Rennes, CNRS, Université de Rennes 1, 35042 Rennes^b, France
⁴⁴INFN, Gruppo Collegato di Trento^a and Università di Trento^b, I-38050 Povo, Trento, Italy; INFN, Sezione di Padova^c and Università di Padova^d, I-35131 Padova, Italy
⁴⁵IM-PAN 00-956 Warsaw^a; Warsaw University 00-681 Warsaw^b; Astronomical Observatory Warsaw University 00-478 Warsaw^c; CAMK-PAN 00-716 Warsaw^d; Białystok University 15-424 Białystok^e; IPJ 05-400 Świerk-Otwock^f; Institute of Astronomy 65-265 Zielona Góra^g, Poland
⁴⁶Rochester Institute of Technology, Rochester, NY 14623, USA
⁴⁷Rutherford Appleton Laboratory, HSIC, Chilton, Didcot, Oxon OX11 0QX United Kingdom
⁴⁸San Jose State University, San Jose, CA 95192, USA
⁴⁹Sonoma State University, Rohnert Park, CA 94928, USA
⁵⁰Southeastern Louisiana University, Hammond, LA 70402, USA
⁵¹Southern University and A&M College, Baton Rouge, LA 70813, USA
⁵²Stanford University, Stanford, CA 94305, USA
⁵³Syracuse University, Syracuse, NY 13244, USA
⁵⁴The Pennsylvania State University, University Park, PA 16802, USA
⁵⁵The University of Melbourne, Parkville VIC 3010, Australia
⁵⁶The University of Mississippi, University, MS 38677, USA
⁵⁷The University of Sheffield, Sheffield S10 2TN, United Kingdom
⁵⁸The University of Texas at Austin, Austin, TX 78712, USA
⁵⁹The University of Texas at Brownsville and Texas Southmost College, Brownsville, TX 78520, USA
⁶⁰Trinity University, San Antonio, TX 78212, USA

- ⁶¹*Tsinghua University, Beijing 100084 China*
⁶²*Universitat de les Illes Balears, E-07122 Palma de Mallorca, Spain*
⁶³*University of Adelaide, Adelaide, SA 5005, Australia*
⁶⁴*University of Birmingham, Birmingham, B15 2TT, United Kingdom*
⁶⁵*University of Florida, Gainesville, FL 32611, USA*
⁶⁶*University of Glasgow, Glasgow, G12 8QQ, United Kingdom*
⁶⁷*University of Maryland, College Park, MD 20742 USA*
⁶⁸*University of Massachusetts - Amherst, Amherst, MA 01003, USA*
⁶⁹*University of Michigan, Ann Arbor, MI 48109, USA*
⁷⁰*University of Minnesota, Minneapolis, MN 55455, USA*
⁷¹*University of Oregon, Eugene, OR 97403, USA*
⁷²*University of Rochester, Rochester, NY 14627, USA*
⁷³*University of Salerno, I-84084 Fisciano (Salerno), Italy and INFN (Sezione di Napoli), Italy*
⁷⁴*University of Sannio at Benevento, I-82100 Benevento, Italy and INFN (Sezione di Napoli), Italy*
⁷⁵*University of Southampton, Southampton, SO17 1BJ, United Kingdom*
⁷⁶*University of Strathclyde, Glasgow, G1 1XQ, United Kingdom*
⁷⁷*University of Western Australia, Crawley, WA 6009, Australia*
⁷⁸*University of Wisconsin-Milwaukee, Milwaukee, WI 53201, USA and*
⁷⁹*Washington State University, Pullman, WA 99164, USA*

The gravitational-wave (GW) sky may include nearby pointlike sources as well as astrophysical and cosmological stochastic backgrounds. Since the relative strength and angular distribution of the many possible sources of GWs are not well constrained, searches for GW signals must be performed in a model-independent way. To that end we perform two directional searches for persistent GWs using data from the LIGO S5 science run: one optimized for pointlike sources and one for arbitrary extended sources. The latter result is the first of its kind. Finding no evidence to support the detection of GWs, we present 90% confidence level (CL) upper-limit maps of GW strain power with typical values between $2-20 \times 10^{-50}$ strain 2 Hz $^{-1}$ and $5-35 \times 10^{-49}$ strain 2 Hz $^{-1}$ sr $^{-1}$ for pointlike and extended sources respectively. The limits on pointlike sources constitute a factor of 30 improvement over the previous best limits. We also set 90% CL limits on the narrow-band root-mean-square GW strain from interesting targets including Sco X-1, SN1987A and the Galactic Center as low as $\approx 7 \times 10^{-25}$ in the most sensitive frequency range near 160 Hz. The limits on Sco X-1 are the most constraining to date and constitute a factor of 5 improvement over the previous best limits. The limits on SN1987A and the Galactic Center are the first of their kind.

Introduction.—One of the most ambitious goals of gravitational-wave (GW) astronomy is to measure the stochastic gravitational-wave background (SGWB), which can arise through a variety of mechanisms including amplification of vacuum fluctuations following inflation [1], phase transitions in the early universe [2], cosmic strings [3] and pre-Big Bang models [4]. Astrophysical sources of the SGWB include the superposition of unresolved sources such as core-collapse supernovae [5], neutron-star instabilities [6], binary mergers [7] and persistent emission from neutron stars [8].

We present the results of two analyses using data from the LIGO S5 science run: a radiometer analysis optimized for pointlike sources and a spherical-harmonic decomposition (SHD) analysis, which allows for arbitrary angular distributions. This work presents the first measurement of the GW sky in a framework consistent with an arbitrary extended source.

Detectors.—We analyze data from LIGO’s 4 km and 2 km detectors (H1 and H2) in Hanford, WA and the 4 km detector (L1) in Livingston Parish, LA during the S5 science run (Nov. 5, 2005 - Sep. 30, 2007). During S5, both H1 and L1 reached a strain sensitivity of 3×10^{-23} strain Hz $^{-1/2}$ in the most sensitive region between 100 – 200 Hz [9] and collected 331 days of coinci-

dent H1L1 and H2L1 data. S5 saw milestones including limits on GWs from the Crab pulsar surpassing those inferred from the Crab’s spindown [10], as well as limits on the isotropic SGWB surpassing indirect limits from Big Bang nucleosynthesis and the cosmic microwave background [11]. This work builds on [11, 12].

Methodology.—Following [12, 13] we present a framework for analyzing the angular distribution of GWs. We assume that the GW signal is stationary and unpolarized, but not necessarily isotropic. It follows that the GW energy density $\Omega_{\text{GW}}(f)$, can be expressed in terms of the GW power spectrum, $\mathcal{P}(f, \hat{\Omega})$:

$$\Omega_{\text{GW}}(f) \equiv \frac{f}{\rho_c} \frac{d\rho_{\text{GW}}}{df} = \frac{2\pi^2}{3H_0^2} f^3 \int_{S^2} d\hat{\Omega} \mathcal{P}(f, \hat{\Omega}). \quad (1)$$

Here f is frequency, $\hat{\Omega}$ is sky location, ρ_c is the critical density of the universe and H_0 is Hubble’s constant. We further assume that $\mathcal{P}(f, \hat{\Omega})$ can be factored (in our analysis band) into an angular power spectrum, $\mathcal{P}(\hat{\Omega})$, and a spectral shape, $\bar{H}(f) \equiv (f/f_0)^\beta$, parameterized by the spectral index β and reference frequency f_0 . We set $f_0 = 100$ Hz to be in the sensitive range of the LIGO interferometers.

We measure $\mathcal{P}(\hat{\Omega})$ for two power-law signal models.

In the cosmological model, $\beta = -3$ ($\Omega_{\text{GW}}(f) = \text{const}$), which is predicted, e.g., for the amplification of vacuum fluctuations following inflation [14]. In the astrophysical model, $\beta = 0$ ($\bar{H}(f) = \text{const}$), which emphasizes the strain sensitivity of the LIGO detectors.

We estimate $\mathcal{P}(\hat{\Omega})$ two ways. The *radiometer algorithm* [12, 15, 16] assumes the signal is a point source characterized by a single direction $\hat{\Omega}_0$ and amplitude, $\eta(\hat{\Omega}_0)$:

$$\mathcal{P}(\hat{\Omega}) \equiv \eta(\hat{\Omega}_0) \delta^2(\hat{\Omega}, \hat{\Omega}_0). \quad (2)$$

It is applicable to a GW sky dominated by a limited number of widely separated point sources. As the number of point sources is increased, however, the beam pattern will cause the signals to interfere and partly cancel. Thus, radiometer maps do not apply to extended sources. Since pointlike signals are expected to arise from astrophysical sources, we use $\beta = 0$ for the radiometer analysis.

The *spherical-harmonic decomposition algorithm* is used for both $\beta = -3$ and $\beta = 0$. It allows for an extended source with an arbitrary angular distribution, characterized by spherical-harmonic coefficients \mathcal{P}_{lm} such that

$$\mathcal{P}(\hat{\Omega}) \equiv \sum_{lm} \mathcal{P}_{lm} Y_{lm}(\hat{\Omega}). \quad (3)$$

The series is cut off at l_{\max} , allowing for angular scale $\sim 2\pi/l_{\max}$. The flexibility of the spherical-harmonic algorithm comes at the price of somewhat diminished sensitivity to point sources, and thus the algorithms are complementary.

We choose l_{\max} to minimize $\sigma(\hat{\Omega}) \bar{A}$ where $\sigma(\hat{\Omega})$ is the uncertainty associated with $\mathcal{P}(\hat{\Omega})$ and \bar{A} is the typical angular area of a resolved patch of sky [27]. I.e., we maximize the sensitivity obtained by integrating over the typical search aperture. We thereby obtain $l_{\max} = 7$ and 12 for $\beta = -3$ and $\beta = 0$, respectively.

Both algorithms can be framed in terms of a “dirty map”, X_ν , which represents the signal convolved with the Fisher matrix, $\Gamma_{\mu\nu}$ [13]:

$$X_\nu = \sum_{ft} \gamma_\nu^*(f, t) \frac{\bar{H}(f)}{P_1(f, t) P_2(f, t)} C(f, t) \quad (4)$$

$$\Gamma_{\mu\nu} = \sum_{ft} \gamma_\mu^*(f, t) \frac{\bar{H}^2(f)}{P_1(f, t) P_2(f, t)} \gamma_\nu(f, t). \quad (5)$$

Here both Greek indices μ and ν take on values of lm for the SHD algorithm and $\hat{\Omega}$ for the radiometer algorithm. $C(f, t)$ is the cross spectral density generated for each interferometer pair. $P_1(f, t)$ and $P_2(f, t)$ are the individual power spectral densities, and $\gamma_\mu(f, t)$ is the angular decomposition of the overlap reduction function $\gamma(\hat{\Omega}, f, t)$, which characterizes the orientations and frequency re-

sponse of the detectors [13]:

$$\gamma_\mu(f, t) \equiv \int_{S^2} d\hat{\Omega} \gamma(\hat{\Omega}, f, t) \mathbf{e}_\mu(\hat{\Omega}) \quad (6)$$

$$\gamma(\hat{\Omega}, f, t) = \frac{1}{2} F_1^A(\hat{\Omega}, t) F_2^A(\hat{\Omega}, t) e^{i2\pi f \hat{\Omega} \cdot (\Delta \vec{x}_{12}(t))/c}. \quad (7)$$

$F_I^A(\hat{\Omega}, t)$ characterizes the detector response of detector I to a GW with polarization A , $\mathbf{e}_\mu(\hat{\Omega})$ is a basis function, c is the speed of light and $\Delta \vec{x}_{12} \equiv \vec{x}_1 - \vec{x}_2$ is the difference vector between the interferometer locations [13].

In [13] it was shown that the maximum-likelihood estimators of GW power are given by $\hat{\mathcal{P}} = \Gamma^{-1} X$. The inversion of Γ is complicated by singular eigenvalues associated with modes to which the Hanford-Livingston (HL) detector network is insensitive. This singularity can be handled two ways. The radiometer algorithm assumes the signal is pointlike, implying that correlations between neighboring pixels can be ignored. Consequently, we can replace Γ^{-1} with $(\Gamma_{\hat{\Omega}\hat{\Omega}})^{-1}$ to estimate the point source amplitude $\eta(\hat{\Omega})$.

The SHD algorithm targets extended sources, so the full Fisher matrix must be taken into account. We regularize Γ by removing a fraction \mathcal{F} of the modes associated with the smallest eigenvalues, to which the HL network is relatively insensitive. By removing some modes from the Fisher matrix, we obtain a regularized inverse Fisher matrix, Γ_R^{-1} , thereby introducing a bias discussed below.

We thereby obtain estimators

$$\hat{\eta}_{\hat{\Omega}} = (\Gamma_{\hat{\Omega}\hat{\Omega}})^{-1} X_{\hat{\Omega}} \quad (8)$$

$$\hat{\mathcal{P}}_{lm} = \sum_{l'm'} (\Gamma_R^{-1})_{lm, l'm'} X_{l'm'}, \quad (9)$$

with uncertainties

$$\sigma_{\hat{\Omega}}^{\text{rad}} = (\Gamma_{\hat{\Omega}\hat{\Omega}})^{-1/2} \quad (10)$$

$$\sigma_{lm}^{\text{sph}} = [(\Gamma_R^{-1})_{lm, lm}]^{1/2}. \quad (11)$$

We refer to $\hat{\mathcal{P}}_{\hat{\Omega}} \equiv \sum_{lm} \hat{\mathcal{P}}_{lm} Y_{lm}(\hat{\Omega})$ as the “clean map” and $\hat{\eta}_{\hat{\Omega}}$ as the “radiometer map.” $\hat{\mathcal{P}}_{\hat{\Omega}}$ has units of $\text{strain}^2 \text{Hz}^{-1} \text{sr}^{-1}$ whereas $\hat{\eta}_{\hat{\Omega}}$ has units of $\text{strain}^2 \text{Hz}^{-1}$.

In choosing \mathcal{F} , we balance the sensitivity to the kept modes with the bias associated with the removed modes. In practice, we do not know the bias associated with \mathcal{F} , which depends on the unknown signal distribution $\mathcal{P}(\hat{\Omega})$. Therefore, we choose \mathcal{F} to produce reliably reconstructed maps with minimal bias for simulated signals. Following [13], we use $\mathcal{F} = 1/3$, which was shown to be a robust choice for simulated signals including maps characterized by one or more point sources, dipoles, monopoles and an extended source clustered in the galactic plane.

The likelihood function for $\mathcal{P}(\hat{\Omega})$ at each point in the sky can be described as a normal distribution with mean $\hat{\mathcal{P}}_{\hat{\Omega}}$ and width $\sigma_{\hat{\Omega}}^{\text{sph}}$. Regularization introduces a signal-dependent bias. Without knowing the true distribution

of $\mathcal{P}(\hat{\Omega})$, it is impossible to know the bias exactly, but it is possible to set a conservative upper limit by assuming that on average the removed modes contain no more GW power than the kept modes. Thus, we calculate $\hat{\mathcal{P}}_{lm}$ setting eigenvalues of removed modes to zero, whereas σ_{lm}^{sph} is conservatively calculated setting eigenvalues of removed modes to the average eigenvalue of the kept modes. These upper limits are $\approx 25\%$ greater than they would be if we used the same regularization scheme for σ_{lm}^{sph} and $\hat{\mathcal{P}}_{lm}$.

In the case of the SHD algorithm, we also calculate [13],

$$\hat{C}_l \equiv \frac{1}{2l+1} \sum_m \left[|\hat{\mathcal{P}}_{lm}|^2 - (\Gamma_R^{-1})_{lm,lm} \right], \quad (12)$$

which describe the angular scale of the clean map. The subtracted second term makes the estimator unbiased so that $\langle \hat{C}_l \rangle = 0$ when no signal is present. The noise distribution of \hat{C}_l is highly non-Gaussian for small values of l , and so the upper limits presented below are calculated numerically. The \hat{C}_l are analogous to similar quantities defined in the context of temperature fluctuations of the cosmic microwave background [17].

The analysis was performed blindly using the S5 stochastic analysis pipeline. This pipeline has been tested with hardware and software injections, and the successful recovery of isotropic hardware injections is documented in [11]. The recovery of anisotropic software injections is demonstrated in [13]. We parse time series into 60 s, Hann-windowed, 50%-overlapping segments, coarse-grained to achieve 0.25 Hz resolution. We apply a stationarity cut described in [12], which rejects $\sim 3\%$ of the segments. We also mask frequency bins associated with instrumental lines (e.g., harmonics of the 60 Hz power, calibration lines and suspension-wire resonances) as well as injected, simulated pulsar signals. For $\beta = -3, 0$ we include frequency bins up to 200, 500 Hz, so that $\sigma(\hat{\Omega})$ is within $\lesssim 2\%$ of the minimum possible value. Thirty-three frequency bins are masked, corresponding to 2% of the frequency bins between 40 – 500 Hz used in the broadband analyses.

In order to determine if there is a statistically significant GW signature, we consider the highest signal-to-noise ratio (SNR) frequency bin or sky-map pixel. We calculate the expected noise probability distribution of the maximum SNR given many independent trials (in a spectral band) and given many *dependent* trials (for a sky map).

For N independent frequency bins, the probability density function, $\pi(\rho_{\max})$, of maximum SNR, ρ_{\max} , is

$$\pi(\rho_{\max}) \propto \left[1 + \text{erf} \left(\rho_{\max}/\sqrt{2} \right) \right]^{N-1} e^{-\rho_{\max}^2/2}. \quad (13)$$

The Gaussianity of $\hat{\mathcal{P}}_{\hat{\Omega}}$ and $\hat{\eta}_{\hat{\Omega}}$, calculated by summing over many $\mathcal{O}(500\text{K})$ independent segments, is expected to arise due to the central limit theorem [18]. Additionally,

we find the Gaussian-noise hypothesis to be consistent with time-slide studies, wherein we perform the cross-correlation analysis with unphysical time-shifts in order to wash out astrophysical signals and thereby obtain different realizations of detector noise.

The distribution of maximum SNR for a sky map is more subtle due to the non-zero covariances between estimators for different patches on the sky. For this case, we calculate $\pi(\rho_{\max})$ numerically by simulating many realizations of dirty maps with covariances described by the Fisher matrix Γ .

Following [11], we marginalize over the H1, H2, and L1 calibration uncertainties [11], which were measured to be 10%, 10%, and 13%, respectively [28]. Using a prior, taken to be flat above $\mathcal{P}(\hat{\Omega}) = 0$, we obtain Bayesian upper limits at 90% CL [29].

Results.—Fig. 1 shows sky maps for SHD $\beta = -3$ (left), SHD $\beta = 0$ (center), and the radiometer $\beta = 0$ (right). The top row contains SNR maps. The maximum SNR values are 3.1 (with significance $p = 25\%$), 3.1 ($p = 56\%$), and 3.2 ($p = 53\%$) respectively. These p -values take into account the number of search directions and covariances between different sky patches. Observing no evidence of GWs, we set upper limits on GW power. The 90% confidence level (CL) upper limit maps are given in the bottom row. For SHD $\beta = -3$, the limits are between $5 - 31 \times 10^{-49} \text{ strain}^2 \text{Hz}^{-1} \text{sr}^{-1}$; for SHD $\beta = 0$, the limits are between $6 - 35 \times 10^{-49} \text{ strain}^2 \text{Hz}^{-1} \text{sr}^{-1}$; and for the radiometer $\beta = 0$, the limits are between $2 - 20 \times 10^{-50} \text{ strain}^2 \text{Hz}^{-1}$. Since the radiometer and SHD maps have different units— $\text{strain}^2 \text{Hz}^{-1}$ and $\text{strain}^2 \text{Hz}^{-1} \text{sr}^{-1}$ respectively—one must scale the SHD map by the typical diffraction limited resolution $\bar{A} \approx 0.1 \text{ sr}$ to perform an approximate comparison.

The strain power limits can also be expressed in terms of energy flux per unit frequency [12]:

$$\hat{F}(f, \hat{\Omega}) = \left(3.18 \times 10^{42} \frac{\text{erg}}{\text{cm}^2 \text{s}} \right) \left(\frac{f}{100 \text{ Hz}} \right)^{\beta+2} \hat{\mathcal{P}}_{\hat{\Omega}}. \quad (14)$$

(Radiometer energy flux is obtained by replacing $\hat{\mathcal{P}}_{\hat{\Omega}}$ with $\hat{\eta}_{\hat{\Omega}}$.) The corresponding values are $2 - 10 \times 10^{-6} (f/100 \text{ Hz})^{-1} \text{ erg cm}^{-2} \text{s}^{-1} \text{Hz}^{-1} \text{sr}^{-1}$ and $2 - 11 \times 10^{-6} (f/100 \text{ Hz})^2 \text{ erg cm}^{-2} \text{s}^{-1} \text{Hz}^{-1} \text{sr}^{-1}$ for the SHD method, and $6 - 60 \times 10^{-8} (f/100 \text{ Hz})^2 \text{ erg cm}^{-2} \text{s}^{-1} \text{Hz}^{-1}$ for the radiometer. The radiometer limits constitutes a factor of ~ 30 improvement over the previous best [12].

Fig. 2 shows 90% CL upper limits on the C_l . Since the $\hat{\mathcal{P}}_{lm}$ have units of $\text{strain}^2 \text{Hz}^{-1} \text{sr}^{-1}$, the C_l have the somewhat unusual units of $\text{strain}^4 \text{Hz}^{-2} \text{sr}^{-2}$.

Sco X-1 is a nearby (2.8 kpc) low-mass X-ray binary likely to include a neutron star spun up through accretion. Its spin frequency is unknown. It has been suggested that the accretion torque is balanced by GW emission [19]. The Doppler line broadening due to the orbital motion is smaller than the chosen $\delta f = 0.25 \text{ Hz}$ bin width

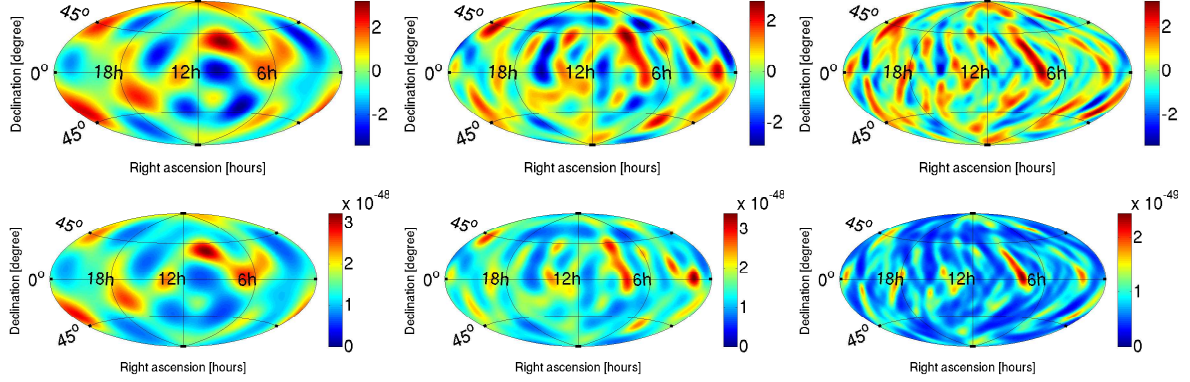


FIG. 1: Top row: SNR maps for the three different analyses: SHD clean map $\beta = -3$ (left), SHD clean map $\beta = 0$ (center), and radiometer $\beta = 0$ (right). All three SNR maps are consistent with detector noise. The p-values associated with each map's maximum SNR are (from left to right) $p = 25\%$, $p = 56\%$, $p = 53\%$. Bottom row: The corresponding 90% CL upper limit maps on strain power in units of $\text{strain}^2 \text{Hz}^{-1} \text{sr}^{-2}$ for the SHD algorithm, and units of $\text{strain}^2 \text{Hz}^{-1}$ for the radiometer algorithm.

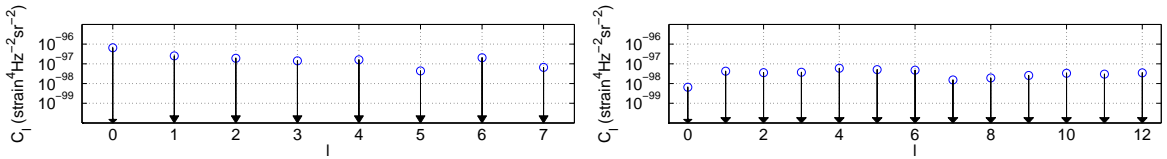


FIG. 2: Upper limits on C_l at 90% CL vs l for the SHD analyses for $\beta = -3$ (left) and $\beta = 0$ (right). The \hat{C}_l are consistent with detector noise.

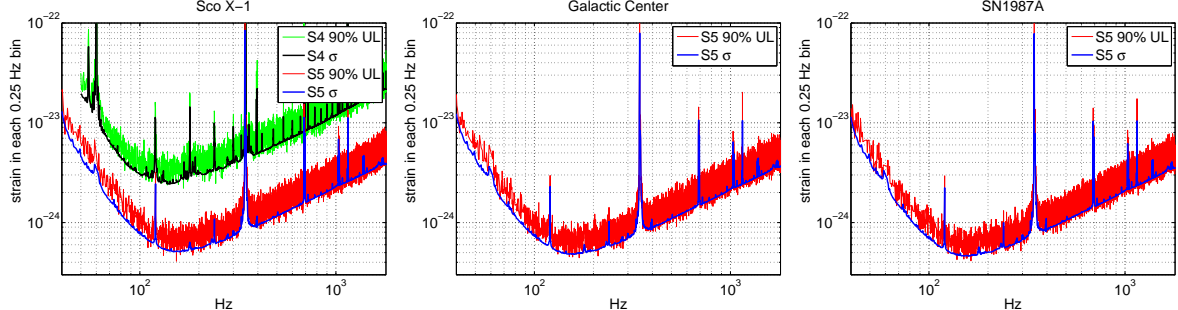


FIG. 3: Radiometer 90% upper limits on RMS strain in each 0.25 Hz wide bin as a function of frequency for Sco X-1 (top-left), the Galactic Center (top-right) and SN1987A (bottom). The large spikes correspond to harmonics of the 60 Hz power mains, calibration lines and suspension-wire resonances. The previous S4 upper limits for Sco X-1 [12] are also plotted in the top-left panel, illustrating the improvement in the upper limits obtained by using the LIGO S5 data. This is the first radiometer measurement of the Galactic Center and SN1987A.

for frequencies below ≈ 930 Hz [20]. At higher frequencies, the signal is certain to span two bins. We determine the maximum value of SNR in the direction of Sco X-1 to be 3.6 ($p = 73\%$ given $\mathcal{O}(7000)$ independent frequency bins) at $f = 1770.50$ Hz. Thus in Fig. 3 (first panel) we present limits on root-mean-square (RMS) strain, $h_{\text{RMS}}(f, \hat{\Omega})$, as a function of frequency in the direction of Sco X-1 (RA, dec) = (16.3 hr, 15.6°). These limits improve on the previous best by a factor of ~ 5 [12]. RMS strain is related to narrow-band GW power via

$$h_{\text{RMS}}(f, \hat{\Omega}) = [\eta(f, \hat{\Omega}) \delta f]^{1/2}, \quad (15)$$

and is better suited for comparison with searches for periodic GWs [21] (see also [22]). These limits apply to a circularly polarized signal from a pulsar whose spin axis is aligned with the line of sight. The limits constrain the RMS strain in each bin as opposed to the total RMS strain from Sco X-1, which might span two bins.

We also look for statistically significant signals associated with the Galactic Center (RA, dec) = (17.8 hr, -29°) and SN1987A (RA, dec) = (5.6 hr, -69°). The maximum SNR values are 3.5 ($p = 85\%$) at $f = 203.25$ Hz and 4.3 at ($p = 7\%$) 1367.25 Hz respectively. Limits on RMS strain are given in Fig. 3.

In summary, no evidence was found to support the detection of either extended or pointlike GW sources. However, the clean maps in Fig. 1 represent the first effort to look for anisotropic extended sources of GWs. With the ongoing construction of second-generation GW interferometers [23–26], we expect to achieve strain sensitivities that will test plausible astrophysical and cosmological models. The new framework presented here is expected to serve as the paradigm for future stochastic analyses.

The authors gratefully acknowledge the support of the United States National Science Foundation for the construction and operation of the LIGO Laboratory, the Science and Technology Facilities Council of the United Kingdom, the Max-Planck-Society, and the State of Niedersachsen/Germany for support of the construction and operation of the GEO600 detector, and the Italian Istituto Nazionale di Fisica Nucleare and the French Centre National de la Recherche Scientifique for the construction and operation of the Virgo detector. The authors also gratefully acknowledge the support of the research by these agencies and by the Australian Research Council, the International Science Linkages program of the Commonwealth of Australia, the Council of Scientific and Industrial Research of India, the Istituto Nazionale di Fisica Nucleare of Italy, the Spanish Ministerio de Educación y Ciencia, the Conselleria d'Economia Hisenda i Innovació of the Govern de les Illes Balears, the Foundation for Fundamental Research on Matter supported by the Netherlands Organisation for Scientific Research, the Polish Ministry of Science and Higher Education, the FOCUS Programme of Foundation for Polish Science, the Royal Society, the Scottish Funding Council, the Scottish Universities Physics Alliance, The National Aeronautics and Space Administration, the Carnegie Trust, the Leverhulme Trust, the David and Lucile Packard Foundation, the Research Corporation, and the Alfred P. Sloan Foundation.

- [2] A. A. Starobinskii, JETP Lett. **30** (1979).
- [3] T. W. B. Kibble, J. Phys. **A9** (1976).
- [4] A. Buonanno, PRD **55** (1997).
- [5] E. Howell et al., MNRAS **351**, 1237 (2004).
- [6] V. Ferrari & S. Matarrese & R. Schneider, MNRAS **303**, 258 (1999).
- [7] T. Regimbau & B. Chauvineaux, CQG **24**, 627 (2007).
- [8] T. Regimbau & J. A. de Freitas Pacheco, A&A **376**, 381 (2001).
- [9] B. P. Abbott et al., Rep. Prog. Phys. **72**, 076901 (2009).
- [10] B. Abbott et al., ApJL **683**, 45 (2008).
- [11] B. Abbott et al., Nature **460**, 990 (2009).
- [12] B. Abbott et al., PRD **76**, 082003 (2007), astro-ph/0703234.
- [13] E. Thrane et al., PRD **80**, 122002 (2009).
- [14] M. Maggiore, Phys. Rept. **331**, 283 (2000).
- [15] S. W. Ballmer, CQG **23**, S179 (2006).
- [16] S. Mitra, S. Dhurandhar, T. Souradeep, et al., PRD **77**, 042002 (2008).
- [17] G. Hinshaw et al., Astrophys. J. Suppl. **180**, 225 (2009).
- [18] B. Allen & J. D. Romano, PRD **59**, 102001 (1999).
- [19] D. Chakrabarty et al., Nature **424**, 42 (2003).
- [20] D. Steeghs & J. Casares, ApJ **568**, 273 (2002).
- [21] B. Abbott et al., PRD **76**, 082001 (2007).
- [22] C. Messenger, *Understanding the sensitivity of the stochastic radiometer analysis in terms of the strain tensor amplitude*, LIGO Document T1000195-v1 (2010).
- [23] G. Harry for the LIGO Science Collaboration, CQG **27**, 084006 (2010).
- [24] J. R. Smith for the LIGO Science Collaboration, CQG **26**, 114013 (2009).
- [25] F. Acernese for The Virgo Collaboration, CQG **23**, S63 (2006).
- [26] K. Kuroda for the LCGT Collaboration, CQG **27**, 084004 (2010).
- [27] The data were first processed with $l_{\max} = 20$; the present method of choosing l_{\max} was then adopted a posteriori to more accurately model the network's angular resolution.
- [28] We follow the marginalization scheme used in [11], but note that this does not take into account covariance between baselines with a shared detector. Because the H2L1 baseline only contributes about 10% of the sensitivity, and the calibration uncertainty is on the order of 10% to start with, this effect is only on the order of 1%. Work is ongoing to take this effect into account.
- [29] A prior constructed from [12] would be nearly flat anyway since the strain sensitivity has improved ten-fold since S4.

^a Electronic address: ethrane@physics.umn.edu

[1] E. W. Kolb & M. S. Turner, *The Early Universe* (Westview Press, 1994).